

Effect of irradiation defects on the plastic slip of $\{112\}$ grain boundary: atomic scale study

N. Kvashin^{a,*}, D. Terentyev^b, A. Serra^a and N. Anento^a

^a*Dept. Civil & Environmental Engineering, Universitat Politècnica de Catalunya, Barcelona, 08034, Spain*

^b*SCK·CEN, Nuclear Materials Science Institute, Boeretang 200, Mol, B-2400, Belgium*

ARTICLE INFO

Keywords:

Grain Boundary Strengthening
Defect Interaction
Grain Boundary Migration
Segregation
Disconnections

ABSTRACT

$\Sigma 3\{112\}$ grain boundary (GB) is known to exhibit plastic slip in bcc metals, which overall contributes to the good ductility and toughness of such metals as iron, matrix element for the steels applied in nuclear industry. During nuclear operation, the neutron irradiation causes formation of point defects and their clusters which lead to the non-equilibrium mass transport and agglomeration of nanoscale defects inside grains and near the grain boundaries. Due to the effect of chemical segregation, GBs can encounter sessile obstacles preventing the GB plastic slip. Understanding the influence of the irradiation defects segregated at the grain boundaries is important for the development of structural steels for nuclear fusion and fission applications. The present paper studies the influence of the irradiation defects, such as Cr precipitates, He bubbles and voids on the plastic slip of the GB interface. The studied defects are found to act as strong obstacles to the glide of the elementary disconnections responsible for the shear-coupled GB migration. The interaction between a single elementary disconnection and a series of them provided by a source has been studied. As a result of the interaction with impenetrable defects the formation of residual defects such as loops is observed.

1. Introduction

Ferritic steels are affordable and reliable materials for structural applications in many domains, including nuclear industry. In the case of this family of materials, high strength and ductility are gained simultaneously thanks to dedicated thermo-mechanical treatment (rolling, forging) and chemical alloying (precipitation as well as solid solution hardening). Grain boundaries play an important role as they provide strength but yet allow controlled plastic deformation to occur homogeneously in the material. Hence, modification of the ductility and strength of grain boundaries due to thermal aging or irradiation damage may degrade those initially attractive mechanical properties

The main mechanism behind plastic deformation of polycrystalline metals is the mobility and multiplication of dislocations [1]. Any obstacle impeding or modifying their motion leads to a change in the mechanical response of the material. One specific mechanism which contributes to the low temperature plastic deformation of metals is the shear-coupled GB migration (SCGBM), as many experiments [2, 3] and molecular dynamics simulations [4, 5] have evidenced. The essential element behind the SCGBM are elementary disconnections, namely, interfacial defects with both dislocation and step character and with high mobility, characterized by the Burgers vector (\mathbf{b}) and the height of the step (h). Their glide along the GB accommodates shear stress and the stepped core displaces the GB interface by transforming one crystal into the other.

Previous atomistic studies performed on several tilt GBs in bcc-Fe [6–9] show in detail the key role played by elementary disconnections on the GB migration and also on the interaction of the GBs with crystal dislocations.

GBs act as sinks for mobile defects, such as point defects and their clusters, created under irradiation conditions [10–13]. **Theoretical and experimental results confirm that nucleation of intergranular helium bubbles, together with chromium precipitation, contribute to intergranular embrittlement in polycrystals [14–18].** In irradiated metals, the interaction between GBs and such defects may happen either thanks to the glide of mobile clusters towards the GB or because a mobile GB encounters defects along its migration process. A fraction of the defects formed as a result of the irradiation may remain immobile, while the rest may be displaced over time to interact with other microstructural defects. The mechanical properties of materials are strongly affected by the evolving microstructure, thus, it is of great importance to study the interaction between such defects and GBs. Atomistic simulation is the most suitable tool to achieve this goal, as it allows a precise treatment of the interaction between both types of defects involved.

Among the tilt GBs present in bcc-Fe, the $\Sigma 3\{110\}$ $\{112\}$ symmetric tilt GB is of special interest as it is the most abundant according to experimental measurements [19]. The $\{112\}$ tilt GB in bcc metals experiences SCGBM. The mechanism is directly applicable to the $\{112\}$ twin boundary and governs the growth and shrinkage of the twin. The elementary disconnections, responsible for SCGBM, can either be created directly

*Corresponding author

✉ nikolai.kvashin@upc.edu (N. Kvashin)

at the pristine interface or, at a lower stress level, by a source of disconnections [6].

One possible source of disconnections is a GB dislocation (GBD) created at the GB as an outcome of the interaction between the interface and a crystal dislocation with Burgers vector $1/2\langle 111 \rangle$. The fact that the crystal dislocation decomposes, in a reversible way, into a GBD that does not step the interface and the disconnection responsible for the motion of the GB is essential to have a conservative process. Thus, the mechanism described accommodates efficiently plastic deformation since no residual defects are left behind in the displacement of the GBs and no atomic diffusion is needed during the whole process.

The study of dislocation interaction with obstacles has been a subject of interest for a long time. Interactions between irradiation defects and dislocations in the bulk have been fully characterized for Fe-based alloys in many studies [20–24]. The nature of dislocation–precipitate interactions is well described by the Orowan mechanism [25]. In contrast, interactions between such defects and GBs are more complex and less understood. Applicability of the Orowan precipitate hardening equation to twin propagation was studied in [26] by two-dimensional dislocation dynamics simulations of a twin tip interacting with a line of obstacles. As for other defects, both voids and He bubbles are considered in a similar way in the literature, despite the fact that the latter shows a slight difference in strength depending on the He amount [27]. Atomic simulations show high shear resistance of such defects leading to strong local interaction [22, 28].

According to the previous studies, spherical irradiation defects can be classified depending on the type of interaction existing between the inner atoms and the incoming linear defects: i) soft defects, also known as shearable defects, when the dislocation interacts effectively with their atoms; ii) hard defects, when the dislocation is not able to interact with the inner atoms because it can not penetrate the defect. Impenetrable defects cannot be sheared by dislocations or disconnections in case of interaction with them.

Interaction with hard defects is consistent with the findings of Richman [29], who suggested that twins in bcc metals could bypass the defects forming a torus shape at the interaction. The hard defect in that case is situated in the inner cavity, and it can be described in terms of disconnection loops. These disconnection loops are equivalent to Orowan dislocation loops that are left behind after the interaction of a bulk dislocation with a non-shearable obstacle [25]. The stress increment due to the defects in the case of interactions with dislocations is given by the **modified formula for Orowan stress**:

$$\Delta\tau_{\text{Orowan}} \sim (Gb/l) [\ln(d^{-1} + l^{-1})^{-1} + B] \quad (1)$$

where G is the shear modulus, b is the magnitude of the

Burgers vector, l is the defect spacing, d is the diameter of the defect, and B is a constant of order 1 [30].

Crystal screw dislocations are able to bypass the defects at high temperatures without direct interaction by shearing. On the other hand, edge dislocations are constrained to their own glide plane, in the same way that disconnections are constrained to the GB interface plane. This is the reason why disconnections are forced to bow around the hard defects leaving a loop on the GB behind the interaction, or to shear them in case of shearable defects. These interesting features of the GB-defect interaction have attracted significant attention of material research at the present time in bcc [31] and hcp [32, 33] metals. In this work we study in detail the interaction of the $\{112\}$ GB and its glissile defects with irradiation defects placed on or near the GB, such as Cr precipitates, voids and He bubbles.

The paper is structured as follows: Section 2 contains a description of the simulation methodology; in Section 3 there are presented the results obtained for the interaction between the GB defects and irradiation defects. Finally, in Sections 4 and 5 the discussion and the main conclusions reached from the results obtained are presented.

2. Methodology

Molecular dynamics simulator LAMMPS [34] has been applied to study the interaction between the $\{112\}$ GB containing an elementary disconnection and a series of irradiation defects. The present atomistic calculations have been performed using supercells containing two grains of bcc iron. The principal axes x , y and z of the upper crystal (λ) were oriented along the $[111]$, $[110]$ and $[\bar{1}12]$ directions, respectively, while the axes for the lower crystal (μ) were mirror reflected. The simulation box consisted of a symmetric bicrystal with an initially coherent symmetric tilt GB interface in the middle. Approximate dimensions of the cell size were $100 \times 60 \times 40$ lattice vectors along the corresponding directions with a total number of atoms ~ 3000000 .

In all performed simulations periodic boundary conditions have been imposed along the y direction (tilt axis). Such approach allows to address the problem as an interaction between the disconnections and row of defects, rather than a single defect, as it was considered in the previous works on dislocation – defects interactions [20, 21, 23, 24, 27].

Each simulation starts with a static relaxation, i.e. energy minimization, which is performed applying fixed boundary conditions along z direction, which is perpendicular to the GB plane. The interatomic interactions in iron are modeled by using the embedded-atom method (EAM) potential developed by G. Ackland *et al.* [35], fitted to reproduce properties of dislocation lines obtained from DFT. In order to model interaction between the bulk iron atoms and atoms of the defects,

two potentials proposed by D. Terentyev *et al.* [36] and by G. Bonny *et al.* [37] are used for the interactions with He atoms and Cr atoms, respectively. A relaxed bicrystal without defects is obtained.

Two different approaches are used in this work. The first approach serves to study the interaction between an irradiation defect placed on a GB with a single disconnection introduced manually. To create the disconnection on the interface, a dislocation core is introduced at the step along the translation vectors between the two grains as described in [31]. **A second approach is used to study the interaction of the defect with several successive disconnections supplied by a source of disconnections. Such said source is obtained as the outcome of an induced interaction between a $1/2\langle 111 \rangle$ crystal dislocation and the $\{112\}$ GB, the details on the reactions can be found in [6]. Once the source is present, we have applied again energy minimization obtaining then the experimental setup where we have introduced each irradiation defect.** All the crystal defects were introduced manually with the use of Atomsk software [39].

Due to a limitation of the molecular dynamics software, for the first approach fixed boundary conditions were also used along the x direction together with the direction perpendicular to the GB plane. This allows to study only a single interaction between the disconnection and the considered irradiation defect.

In order to study the effect of the relative position GB-defect on the interaction, two different initial positions of the defects were used. The first one is directly on the interface with the center of the defect placed at the GB plane, and the second one is 5 Å above the interface. The distance the GB moves once the disconnection passes along the interface is equal to the height of the step of the disconnection, which is $1/6\langle 112 \rangle a_0 \sim 1.2\text{Å}$. Several sizes have been considered for the defects which were chosen to be the same for voids, precipitates and He bubbles, ranging from 0.25 to 5 nm in diameter.

Concerning to the introduction of irradiation defects, voids were introduced by simply removing atoms located in a spherical region with a given position and size. Helium bubbles were introduced by inserting He atoms in place of voids with the ratio of two He atoms per one vacancy. And as for precipitates, three different orientations of the inner atomic planes were studied. Since chromium shares the same bcc structure of the matrix, the atoms of the precipitate are also oriented in a specific way. Three different cases have been considered: 1) atomic planes in the precipitate are oriented in the same way as the removed iron atoms (direct replacement of Fe atoms by Cr atoms considering the difference in lattice parameters) – tagged as 'subst' or referred to simply as precipitates; 2) atomic planes in the precipitate are oriented in the same way as the Fe planes in the λ grain – identified as

'112'; 3) atomic planes in the precipitate are oriented along [100], [010] and [001] directions – named '100'. Both '112' and '100' precipitates represent extreme cases to study the effect of interaction at the edge of the defect.

Two types of simulations were performed: (i) molecular static to study the interactions in detail as an extreme case at $T = 0$ K and (ii) molecular dynamics at $T = 300$ K to study the effects of temperature on the reaction and the stress level required to trigger it. In both cases an incremental shear strain was applied in order to move the disconnection towards the irradiation defect to initiate the interaction between them. The stress state of the system is recorded after each increment of strain and the open visualization tool OVITO is used for visualization and analysis of atomistic simulation data [40].

3. Results

In this Section we present the main results obtained on the interaction between the $\{112\}$ GB and different irradiation defects providing a description of the reactions observed, depending on a variety of parameters. Initially, we describe the interaction of a single disconnection with irradiation defects of different size placed on the interface via molecular static simulations. In the following subsections we investigate the effect of several factors on this interaction: temperature, relative position of the defect and number of disconnections.

3.1. Size effect on interaction with a single disconnection

In the present Section we focus on the static interaction ($T = 0$ K) between an irradiation defect and a single disconnection previously inserted on the GB.

Fig. 1 shows cases of shear stress versus strain curves for voids and bubbles of different diameters. **We can notice that all the curves share the same trends: in the linear elastic region there are small drops of 3 MPa (inset in Fig. 1a) which happens when the disconnection glides a distance equivalent to its B_v ($\sim 0.29a_0$). The disconnection motion cannot accommodate all the stress supplied, which leads to an increase of the total stress in the system. When the disconnection interacts with the defects at around 0.005 applied strain, there is a release of around 90–120 MPa.**

The full process of interaction between a spherical irradiation defect and a disconnection is qualitatively similar to the interaction between these defects and a crystal dislocation. It can be divided into four stages shown in Fig. 1 as follows: (1) the disconnection glides freely towards the defect; (2) the disconnection reaches the defect and gets attached to it; (3) as the stress increases, the shape of the disconnection changes in two possible ways: for hard defects it remains attached

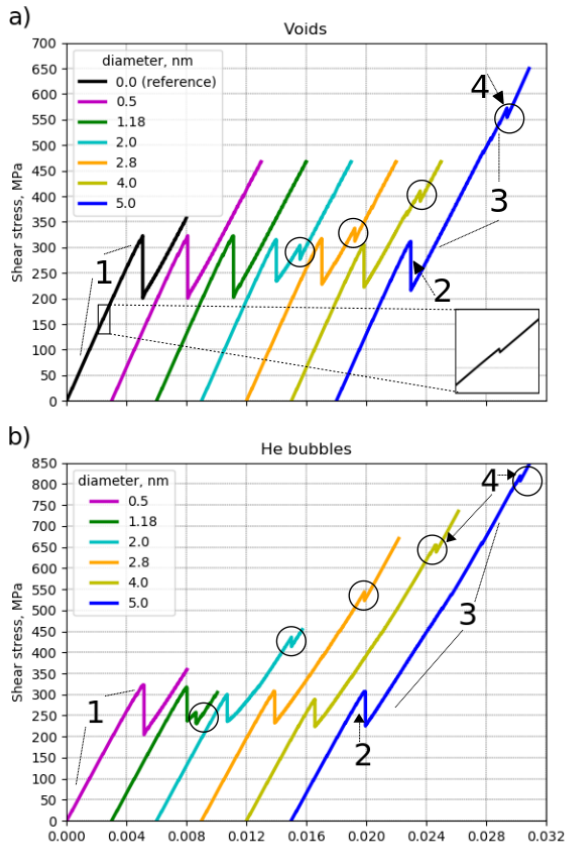


Figure 1: Shear stress vs strain applied in static simulations with voids and bubbles of different sizes placed on the interface. The colors correspond to different diameters in nm. Interactions with rows of a) voids; b) He bubbles. Marked with '1' and '3' are the parts with linear increase of stress in the system, while drops at '2' and '4' correspond to the interaction between the disconnection and the defect and the break away of the disconnection, respectively. The critical stresses marked as '4', highlighted with circles, are plotted in Fig. 3. For the readability purpose the curves are offset from each other along x axis by 0.003.

to their edge, while for soft defects the disconnection interacts with their inner atoms changing the shape of the defect; and (4) the disconnection totally overcomes the defect and breaks away.

Let's now present each stage of the interaction in full detail. Before the attachment of the disconnection to the defect there is a linear part of the curve corresponding to the glide of the disconnection (region marked as '1' in Fig. 1). Although the presence of the defect does not affect significantly the elastic properties of the material, increasing the size of the defect causes a slight reduction in the shear modulus.

When a certain size threshold is exceeded the defects act as strong obstacles for the glide of disconnections. For the smallest sizes, defects are transparent for the motion of the disconnection, i.e. there is no

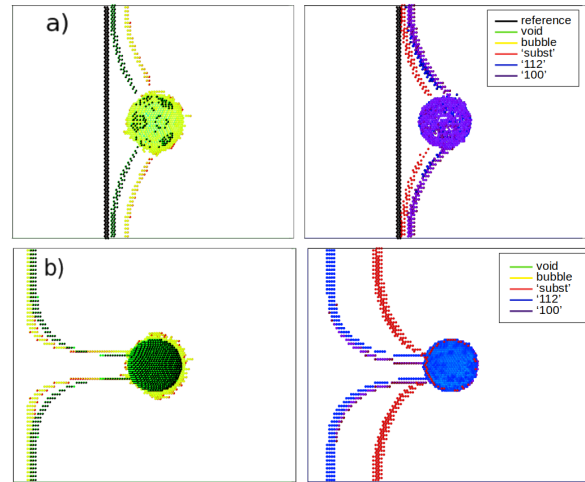


Figure 2: Snapshots from the simulations of the 5 nm diameter defects on the interface interacting with the single disconnection. a) Top projections showing the shapes of the disconnection attached to the defect. Reference case is shown in black. b) Snapshots from the same simulations at the critical stress, i.e. critical line shapes.

attachment to the defect (compare the black curve in Fig. 1a with purple curves in Fig. 1a, 1b). Indeed, the smallest void consists only of five vacancies. For the bigger defects, once reached the required stress level, it attaches to the defects bending its line (see drop of stress marked as '2' in Fig. 1). The attachment allows further concentration of stresses at the defects interaction site, while bowing the disconnection line (region marked as '3' in Fig. 1).

The type of the precipitates used in the study of the size effect is the 'subst' one, i.e. without incoherent boundary at the edge. Such precipitates act as transparent obstacles, i.e. the disconnection is not pinned at the edge. In order to investigate the interaction process when the disconnection is attached to the precipitate, additional cases were modeled – 'subst', '112' and '100' with a 5 nm diameter. In doing so, we obtain the configuration with pinned disconnections as shown in Fig. 2a.

The final stage takes place when the system accommodates enough stress for the disconnection to break away, reflected as drops of of 20–30 MPa in the stress-strain curve (marked as '4' in Fig. 1). Note that for the smallest transparent defects there is no such release of stress, it is included in the drop at 0.005 of applied strain. Fig. 2b shows the critical line shapes for disconnections passing a certain defect right before the break away of the disconnection. Comparing it with the Fig. 2a we can see how the defects interaction changes shape of the line accommodating stress along with it. Disconnections interacting with '100' and '112' precipitates have similar shapes before detachments. The disconnections pass almost the same distance for

both cases, as the critical stresses before detachment for these precipitates are similar. Disconnection is detached from 'subst' precipitate at the lowest strain applied since the precipitate keeps the same orientation as the bicrystal. There are only interactions involving the interface between two metals. All three types of precipitates, together with voids, can be considered as soft obstacles, as no residual defects are left on the interface, and the inner atoms of the defects are found to be sheared (see Fig. 6).

As for Helium bubbles, the He-He and He-Fe interactions are repulsive [36], leading to an increase of the value of the critical stress and subsequently, to an extension of the critical shape. The disconnection line encircles the bubble without affecting the inner atoms, therefore, bubble act as a hard obstacle.

Comparing the results of the present study with the ones presented in [21, 22] on the interaction between edge dislocations and voids we notice a qualitative agreement between both. This similarity can be explained by the fact that both, dislocations of [21, 22] and disconnections, share the same edge character differing only on the Bv magnitude ($0.87a_0$ vs $0.29a_0$). And it allows to perform an estimation of the critical stress of void strengthening in the same way described in eq. (1). In our study $b = 0.87a_0$ is the Bv magnitude of the shortest possible edge dislocation. The dependence of the critical stress as a function of the harmonic diameter for the different defects is plotted in Fig. 3 along with the value predicted from eq. (1) with values of B taken from [21, 22].

Atomic simulations of dislocation – void interaction showed that the possibility of a dislocation climb reduces the strength of the void, as the size of the void is decreased. However, in the case of disconnections, their glide is strictly limited to a single $\{112\}$ plane, showing a good agreement between the theoretical values and simulation data on voids.

He bubbles affect not only the elastic properties, but the crystallographic interaction between the defects, increasing the critical stress. The disconnection interacts with the bubble forming a screw disconnection dipole, which contributes to distribution, yet the values predicted from eq. (1) fit the simulation results. The extra resistance for the largest bubbles, with the size exceeding 3 nm, likely comes from the large spacing of the dipole arms, because the disconnection is not absorbed inside the bubble unlike inside the void. According to the best fit, $B = 1.52$ provides good agreement for the breakaway stress between MD and eq. (1).

Precipitates act as transparent obstacles if the disconnection is not pinned to the defect. This pinning only happens when the size of the precipitate is the highest considered (diameter of 5 nm). For the latter, once the disconnection is attached to the defect, there is a stress threshold that must be reached for the

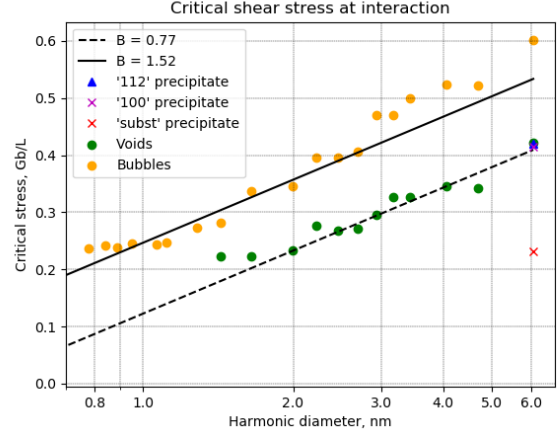


Figure 3: Critical stress for the detachment of the disconnections from different defects as function of harmonic diameter of an obstacle.

disconnection to be able to overcome the incoherencies at the edges of the defect. At this, the resistance of the coherent ('subst') precipitate is essentially smaller as compared to the precipitate with the core structure different from the interface orientation. The extra resistance can naturally be explained by the additional work required to shear the precipitate in the non-favorable plane. The reason for low and negligible resistance of small precipitates needs to be studied further.

In the next Sections we introduce a new element in the simulations: a source of disconnections. As it has been explained in the Introduction Section, this source is capable to produce continuously a flow of disconnections which interact with the irradiation defects. One of the relevant differences with respect to the single disconnection case is the level of stress in the system. The GBD acting as a source in our simulations can produce a dipole of disconnections when the stress level is around 2.2 GPa, while the stress needed for a single disconnection to glide is around 20 MPa [6, 31]. At the stress level required for the source of disconnections in our simulations, the behavior of the defect does not affect the stress distribution and the reaction outcome. The results show a very different behavior that the one described in this Section, evidencing that the interaction of each disconnection with a given defect is heavily influenced by the next incoming disconnections.

3.2. Static interactions with several disconnections

In the present Section we show the details of the interaction between the same set of irradiation defects introduced in Section 3.1 and disconnections supplied continuously by a source. Both, static and dynamic cases, are studied for each defect and initial relative position, namely on and above the GB interface. For

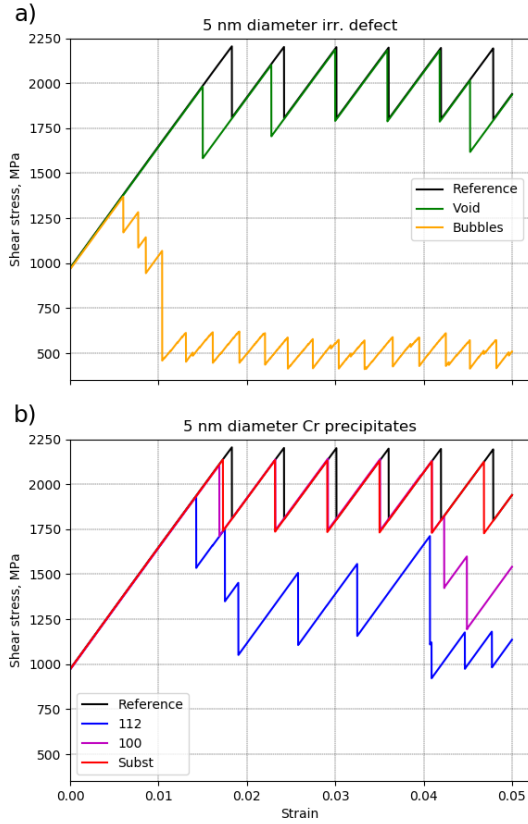


Figure 4: Shear stress vs strain applied in static simulations with defects of extreme size placed on the interface. a) Curves for void and bubble; b) curves for precipitates. The colors' meaning is the same as before.

the sake of interest, we have only considered defects of extreme sizes, i.e. 5 nm in diameter.

A GBD formed at the interface as a result of the absorption of a crystal edge dislocation acts as a stress concentrator. Once the critical stress is reached, a dipole of disconnections is emitted. When the emission of disconnections takes place, there is a release of stress around 400 MPa and the interface is displaced one $\{112\}$ atomic plane, i.e. $0.408a_0 \sim 1.2\text{\AA}$.

Fig. 4 shows the shear stress averaged over all mobile atoms versus the strain applied for all defects studied in static simulations, when the defects are placed on the interface. The result for voids seems to indicate that these defects have little to none effect on the gliding of disconnections (green line in Fig. 4a), therefore voids act as soft defects. The difference between the shear stress needed for creation of a disconnection dipole (2.2 GPa, see black curve in Fig. 4) and the critical shear stress for the void of the extreme size (0.57 GPa, see blue curve in Fig. 1a) explains the observed transparency of the void to the glide of disconnections.

On the contrary, helium bubbles have a significant effect on the shear stress (yellow line in Fig. 4a) and the

propagation of disconnections along the interface. After the initial emission of four disconnections, a steady state is reached at around 0.6 GPa. This level of stress is about 0.2 GPa lower than the critical stress for the interaction between the bubble of extreme size with a single disconnection (0.82 GPa, see blue curve in Fig. 1b). In our simulations we have established a ratio of 2 to 1 between He atoms and vacancies in the bubbles, which are considered as over-pressurized according to [27] and consequently, should behave as weaker obstacles than bubbles with a smaller ratio.

The interaction of the first disconnection with the bubble shows remarkable differences with the process described in Section 3.1: in order to minimize the intersection between both defects (accompanied by a reduction of the maximum shear stress) an interstitial cluster is emitted. Simultaneously, it takes place a pile-up of the subsequent disconnections, leading to the formation of residual disconnection loops around the bubble prior to closing of screw disconnection segments followed by detachment (see Fig. 5).

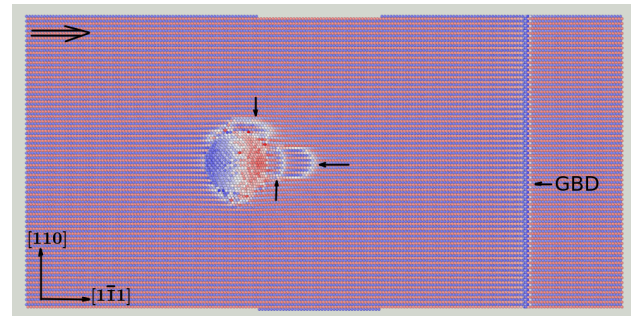


Figure 5: Snapshots from the simulations showing the top projection of the He bubble case after a drop of 0.61 MPa at 0.01 applied strain shown in Fig. 4a – disconnection is detached and absorbed by the GBD, leaving residual loops, shown by small black arrows. Big arrow in the top left corner shows the direction of the disconnection motion.

As for the Cr precipitates, our results for the 'subst' and '100' configurations prove that propagation of the disconnections seems to be unaffected by the internal structure of the defect, as the level of the critical stress measured for both cases is the same, around 2.2 GPa, which is significantly higher than the measured values for the single disconnection case ($0.75Gb/l = 0.32$ GPa for 'subst' and $1.31Gb/l = 0.56$ for '100' from the Fig. 3). At such level of stress the inner structure of the precipitate does not affect the reaction, as the disconnections cross through the precipitates as if they were transparent obstacles. As the GB moves up, the effective size of the defect is progressively reduced, up to the point that disconnections interact only with the tip of the defect. For '100' precipitates we observed that Cr atoms are sheared by the disconnections.

The behavior observed for '112' precipitates indicates that disconnections interact with the inner

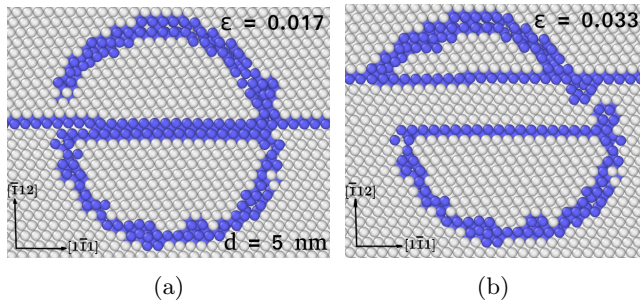


Figure 6: Snapshots from the simulations showing side projections of the '112' Cr precipitate at different strains applied. White atoms correspond to atoms in perfect bcc positions, while blue atoms correspond to disturbed crystal structure.

atoms of the defect, changing the orientation of its atomic planes. The stress state for the '112' case is different as it is sheared by the disconnections. The first disconnection crossing through leaves a stacking fault inside the precipitate, shown on Fig. 6a. When the subsequent disconnections cross the defect the interface moves up, inducing the creation and growth of a 'twin-like' structure inside the precipitate. The lower part of the precipitate keeps the initial orientation and the form, while the upper part is reoriented as the lower grain. Fig. 6b shows the configuration after 10 disconnections have crossed through the defect.

With the purpose of analyzing the effect of the GB-defect relative position on the interaction, we have carried out a new set of simulations placing the defects three atomic planes above the interface. The main difference with respect to the previous experimental setup is the effective size of the interaction. For all the defects considered, once the interface reaches the edge of the defect, the disconnections interact with it as a hard obstacle. At higher strains applied, when the effective size increases, the defects behave the same way as in the former case of defects placed on the interface.

Static simulations allow us to see the mechanisms of interactions. Depending on the defect type, disconnections can either interact with internal atoms of the defects or pass along the defect surface. The relative position of the defect is immaterial, as it does not affect the outcome of the interaction.

3.3. Dynamic interactions with several disconnections

For the simulations at a finite temperature the system was relaxed after the introduction of the defects, thermalized for 25 ps, then a deformation with a constant strain rate $\dot{\epsilon} = 5 \times 10^7 \text{ s}^{-1}$ was applied. Emission and glide of disconnections release more stress than in static simulations. For instance, in the reference case emission of disconnections starts at the very beginning of strain application. Because of the presence of the source of disconnections on the interface, the initial stress state is different from zero, but it is around 0.8

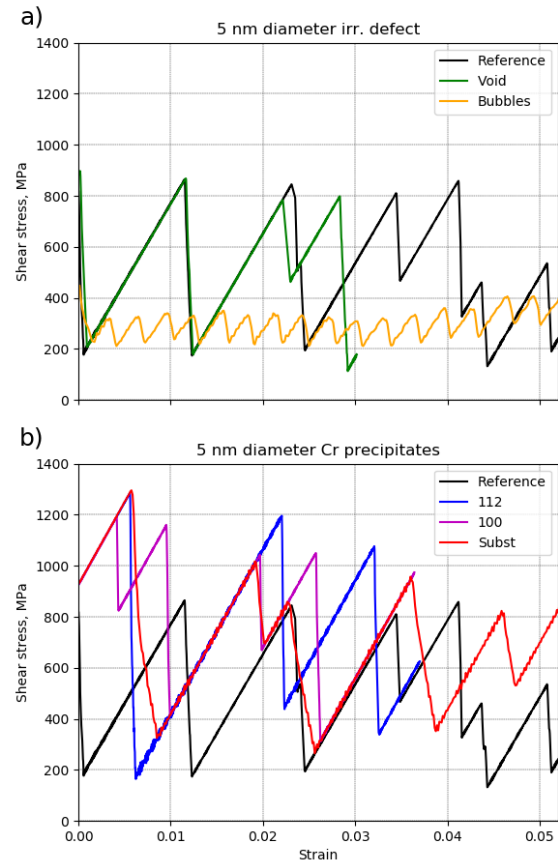


Figure 7: Shear stress vs strain applied in dynamic simulations at 300 K with defects of extreme size placed on the interface. a) Curves for void and bubble; b) curves for precipitates. The colors' meaning is the same as before.

GPa. This stress level is enough to trigger an emission of a disconnection dipole (black line in Fig. 7a). This state is steady, i.e. every time the system reaches this level of shear stress, there is an emission of a dipole, which releases around 0.65 GPa.

In the case of voids, there are few differences between the static and dynamic cases (green line in Fig. 7a). The shear stress curves are similar to the reference case curves. Local stress concentrations affect the shape of the disconnection line and the actual stress in the system, but not the reaction and the final outcome. There are no residual defects left attached to the void after the interaction.

As for the Cr precipitates, dynamic simulations show a similar interaction process, irrespective of the GB-defect relative position. The shear stress needed to trigger the first reaction for the precipitates on the GB is around 1.3 GPa for 'subst' and '112' cases and around 1.2 GPa for '100' case. These values are two times lower than the equivalents from the static simulations (compare Fig. 4b and Fig. 7b). Once this stress level is reached, the GBD emits sequentially six disconnections.

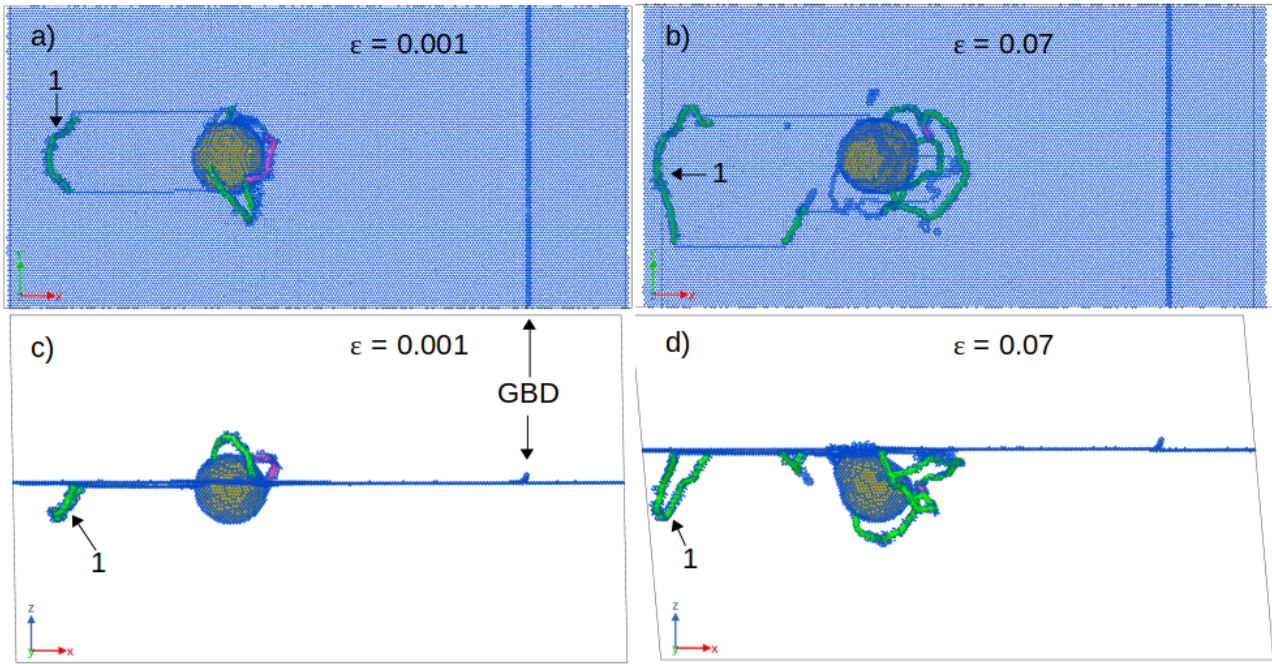


Figure 8: Snapshots from the simulations of He bubble on the interface. Top projections at a) 0.001 strain applied and at b) 0.07 of strain applied. Side projections at c) 0.001 strain applied and at d) 0.07 of strain applied. Marked as '1' is the dislocation loop growing into the lower grain. Blue atoms correspond to Fe, yellow atoms correspond to He. Dislocation loops are indicated with colored lines according to their Bv: green is $1/2\langle 111 \rangle$, while pink is $\langle 100 \rangle$.

After that the disconnections interact with precipitates as soft transparent obstacles.

Once again, Helium bubbles present the most complex interaction mechanism of all defects considered in this study. Once the first disconnection crosses through the bubble, which acts as a hard obstacle, an interfacial loop is created. The shear stress level when detachment of the disconnection takes place is the lowest among all the measurements. Once at least three disconnections interact with the bubble, a creation of a dislocation loop attached to the interface is possible. Its Bv is the sum of the Bv of the three disconnection loops: $1/2\langle 111 \rangle = 3^{1/6}\langle 111 \rangle$, and the height of the step allows the motion of the loop outside the GB plane. This happens for both positions of the bubble. The system reaches steady state at around 0.33 GPa (Fig. 7a), at which single disconnections are detached from the bubble releasing around 0.1 GPa. **Along with every interaction, the length of the dislocation loop growing in the lower grain increases. After the interaction with the first two disconnections, the length is 94.7 Å (marked as '1' in Fig. 8a,c), and 190 Å at the end of strain application (marked as '1' in Fig. 8b,d).**

An overview of the dynamic results shows that applying temperature lowers the stress accumulated in the system, as the stress threshold to initiate the emission of disconnections is significantly lower than for $T = 0$ K. However, the level of stress is high enough for the disconnection to not interact with the defects as strong obstacles. Changing the GB-defect

relative position seems to have a negligible effect on the interaction process, as it only implies a change in the effective size of the defect interacting with the disconnections. This size increases for the defects placed above the interface after the attachment of the defect to the GB, and decreases for the defects placed on the interface, as the GB moves up.

4. Discussion

The elementary disconnections of the $\{112\}$ GB are highly mobile, producing the displacement of the GB along a direction normal to its interface. The step height of the elementary disconnection is just one atomic plane, which means that no shuffles occur and these disconnections glide easily under a relatively low critical resolved shear stress (around 20 MPa in pure Fe). This property is in the basis of the motion of the $\{112\}$ GB. One particular feature of this interface is that when a single edge dislocation interacts with the $\{112\}$ GB a GBD is created, which acts as a source of elementary disconnections. This source plays a relevant role on the evolution of the $\{112\}$ GB because the level of stress it requires for the emission of a disconnection dipole is significantly lower than for the pristine interface, therefore it becomes the preferred mechanism for SCGBM. Since this GB is highly mobile, it can interact with sessile irradiation defects found on the interface or on its vicinity, as GBs are natural sinks for irradiation point defects and mobile defect clusters.

In static simulations of the interaction between a single disconnection with different defects the stress level is not affected by the presence of the other defect regardless of its type. All the irradiation defects studied act as strong obstacles to the motion of a single disconnection. The size of the defect defines the critical value for the disconnection detachment, as well as the defect behavior. Both, the inner structure of the defect and the matrix-defect interface, affect the propagation of the disconnections and the critical stress required to cross through the defect. Table 1 presents the details on shear stresses for all studied defects with a 5 nm diameter (extreme size) upon interaction with a row of disconnections. Comparing these results with the ones for interaction with a single disconnection, we can notice that the values of the normalized stress appear to be rather larger compared to the values from the curves in the Fig. 3. This difference can be understood as a consequence of the higher stress needed to activate the emission of a disconnection dipole by the GBD. As for the discrepancies observed with respect to the stress level on the interaction with crystal dislocations [20–24, 27], these can be determined by the inability of the disconnections to climb.

Table 1
Critical stresses (Gb/l) for the extreme size defects.

Defect type	On GB, 0K	On GB, 300K	Above GB, 0K	Above GB, 300K
Reference	1.89	0.73	-	-
Void	1.72	0.75	1.89	0.64
He Bubble	0.51	0.28	0.39	0.17
'100' Prec	1.80	1.03	1.85	1.12
'112' Prec	1.63	1.12	1.85	1.12
'Subst' Prec	1.85	1.12	1.84	1.12

When the disconnections are supplied by the GBD, the stresses in the system are substantially higher, so that disconnections cross through the defects as if these were transparent obstacles. In this case the defects interact with several consecutive disconnections, and the influence of each defect is noticeable: i) voids do not contribute to the stress redistribution, as the level of stresses is similar to the reference cases; ii) Cr precipitates increase the total stress content in the system, thanks to the chromium admixture, therefore the chromium potential contributes to the stress; iii) Helium bubbles are the only defects that act as Orowan-like obstacles, inhibiting the initial motion of the disconnections supplied by the source. Despite that they reduce the stress needed to displace the GB one plane.

Applying temperature allows the reduction of the stress needed to trigger the reaction (Table 1). When a high strain rate is used the system is not allowed to accommodate the deformation uniformly as it happens

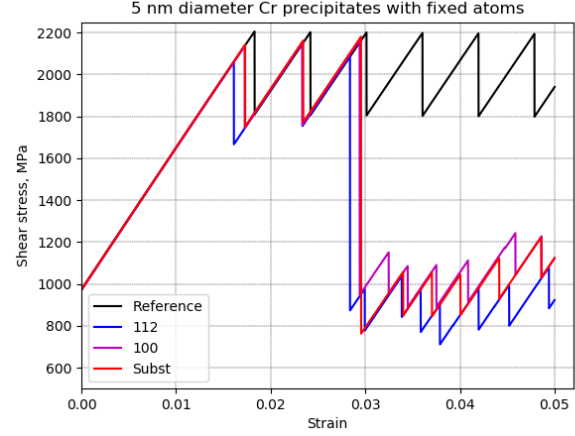


Figure 9: Shear stress vs strain applied in static simulations with precipitates of fixed Cr atoms placed on the interface. Colors meaning is the same as before.

on a relaxation process, leading to the formation of residual disconnection loops and dislocation loops attached to the GB and irradiation defects.

In order to exclude the effects of the interaction between two metals for the precipitates case, one can study the configuration with the precipitates atoms held fixed during the whole loading process. This constraint forbids the crystallographic interactions between the disconnections and the atoms inside the precipitates. Instead, the disconnections pass along the surfaces of the defects, as in He bubble case, i.e. precipitates can be considered as hard defects in this case.

Fig. 9 shows the shear stress – strain curves for the precipitates placed on the interface. The saw-tooth region of the curve after the linear part corresponds to the interaction of the disconnections emitted by the GBD with the tips of the precipitates without any residual defects outside the GB interface, similarly to the previously described cases. The steady state part is followed by a huge drop of stress of around 1.2 – 1.4 GPa. This drop corresponds to the formation of residual defects – dislocation loops – at the Cr-Fe interface similar to the case of the interaction with bubbles (see Fig. 10). These loops stay attached to the GB interface. While the part released into the bulk is able to move under external load, the parts attached to the precipitate increase in length only along with the interaction between the precipitate and a disconnection.

5. Concluding remarks

The existence of highly mobile disconnections specific to the $\{112\}$ GB, which are responsible for shear-coupled GB migration allows the interaction between such GB and radiation induced defects segregated at

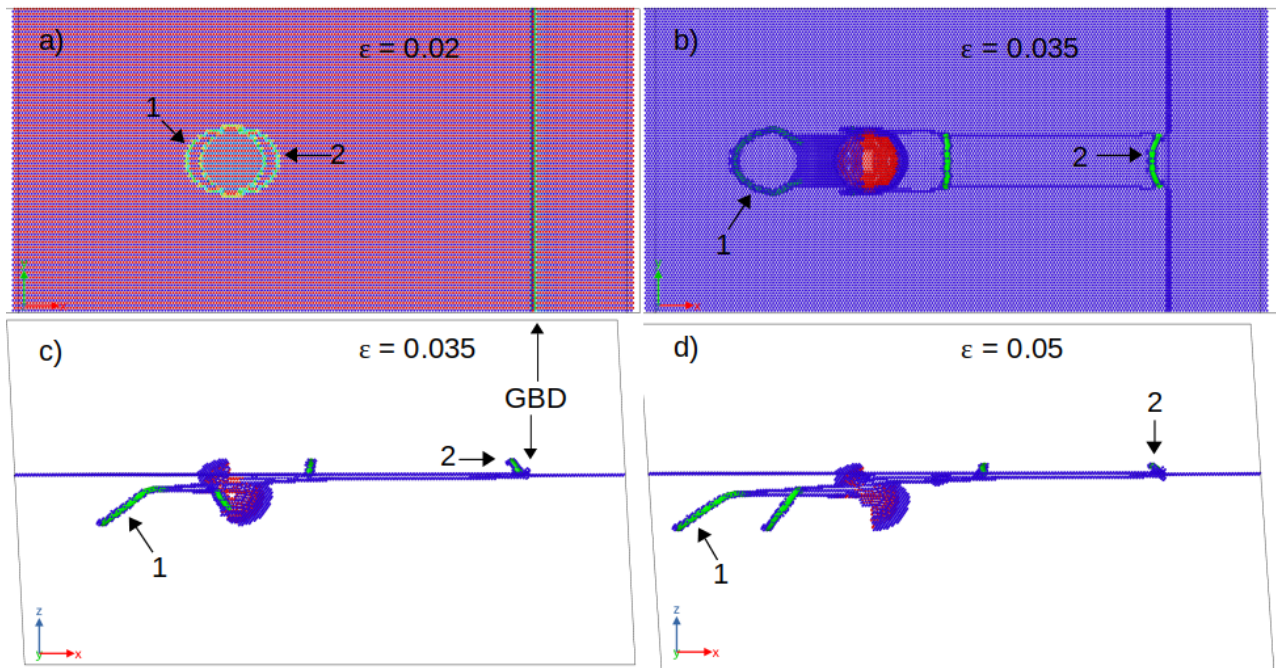


Figure 10: Snapshots from the simulations of Cr 'subst' precipitate with fixed atoms on the interface. Top projections on a) at 0.02 strain applied and on b) at 0.035 of strain applied. Side projections on c) at 0.035 strain applied and on d) at 0.05 strain applied. On a) disconnection loops attached to the precipitate are shown (atoms are colored to distinguish the defects); on b), c) and d) several dislocation loops attached to the GB and the precipitate are shown (blue atoms correspond to Fe, while red atoms correspond to Cr). Marked as '1' and '2' are the initial disconnection loops on a) that grow into dislocation loops in the lower grain and b), c) and d).

the interface or in its vicinity. The interaction of the GB with a crystal dislocation produces a GBD, which is a source of such disconnections, lowering the critical level of stresses needed to start the motion of the GB.

The purpose of the present work is to investigate the interaction between the mobile disconnections of the $\{112\}$ GB and irradiation defects. The main objectives of the work can be summarized as follows:

- The description of the interaction mechanisms in terms of changes in the B_v and the final outcome of the reaction.
- The calculation of the stress required to detach the disconnections from the irradiation defects.
- The description and comparison of the results obtained using the formalism developed in earlier works for crystal dislocations.

Depending on their type, irradiation defects can be considered either as hard obstacles – their inner structure is not affected by the glide of disconnections, i.e. impenetrable obstacles (He bubbles), or soft obstacles – their atoms interact with the disconnections changing the shape/structure of the defect, i.e. being sheared (Cr precipitates, voids). The behavior of the defect is directly reflected in both, the critical stress required to overcome the defect and the reaction mechanism involved. For example, the interaction with He

bubbles may lead to the generation of disconnection loops (analogy of shear loops in the case of bulk dislocation interaction with impenetrable obstacles).

The response of the voids shows a good agreement with the theoretical prediction of the modified Orowan relation for void-crystal dislocation interactions.

For the studied defects, no drag by the moving GB is found. When the GB interface passes through the soft defect, its shape is transformed according to the orientation of the grain where it is situated.

The main effect of temperature is the reduction of the stress needed to trigger the reaction, as expected.

The reactions between the disconnections and the irradiation defects obey two scenarios. At low stresses in the system, the disconnection is attached to the defect independently of its type; with the increase of strain applied it is detached once the critical level of stress is reached. At higher stresses the disconnections pass the defect almost as a transparent obstacle implying that the friction stress is already so high that the additional contribution coming from the defects is negligible.

Altogether the studied defects do affect the propagation of the disconnections and the corresponding plastic slip of the GB. Hence, the presence of the irradiation defects at GBs should lead to the overall hardening of the material. Such hardening should in

turn translate into the suppression of the plastic deformation near the grain boundaries and accumulation of stress concentration eventually causing intergranular fracture. This study reveals a lot of similarities between the interaction mechanisms observed for GB disconnections and observed for standard bulk dislocations [21, 22, 27]. Although further studies are required to investigate other types of GBs, the applicability of the currently established dislocation theory at least extends for the studied $\{112\}$ GB interface.

CRedit authorship contribution statement

N. Kvashin: Methodology, Software, Formal analysis, Investigation, Writing - Original Draft. **D. Terentyev:** Conceptualization, Methodology, Software, Writing - Reviewing and Editing, Funding acquisition. **A. Serra:** Conceptualization, Writing - Reviewing and Editing, Formal analysis, Supervision. **N. Anento:** Writing - Reviewing and Editing, Software, Funding acquisition, Supervision.

Declaration of Competing Interest

The authors declare that they have no known competing financial interests or personal relationships that could have appeared to influence the work reported in this paper.

Acknowledgments

This work was supported by the Euratom research and training programme 2014-2018 under grant agreement No 755039 (Project M4F). This work is partially sponsored by Belgium FOD fusion grant.

Data availability

The raw/processed data required to reproduce these findings cannot be shared at this time as the data also forms part of an ongoing study.

References

- [1] P. Anderson, J. Hirth, J. Lothe, Theory of Dislocations, 3rd ed. ed., Cambridge University Press, Cambridge, 2017.
- [2] T. Gorkaya, D. Molodov, G. Gottstein, Stress-driven migration of symmetrical $\langle 100 \rangle$ tilt grain boundaries in al bicrystals, *Acta Mater.* 57 (2009) 5396–5405.
- [3] A. Rajabzadeh, M. Legros, N. Combe, F. Momprou, D. A. Molodov, Evidence of grain boundary dislocation step motion associated to shear-coupled grain boundary migration, *Philos. Mag.* 93 (2013) 1299–1316.
- [4] J. Cahn, Y. Mishin, A. Suzuki, Coupling grain boundary motion to shear deformation, *Acta Mater.* 54 (2006) 4953–4975.
- [5] H. Khater, A. Serra, R. Pond, J. Hirth, The disconnection mechanism of coupled migration and shear at grain boundaries, *Acta Mater.* 60 (2012) 2007–2020.
- [6] N. Kvashin, P. García-Müller, N. Anento, A. Serra, Atomic processes of the shear-coupled migration of $\{112\}$ twins and vicinal grain boundaries in bcc-Fe, *Phys. Rev. Mat.* 4 (2020) 073604.
- [7] N. Kvashin, N. Anento, D. Terentyev, A. Bakaev, A. Serra, Interaction of a dislocation pileup with $\{332\}$ tilt grain boundary in bcc metals studied by MD simulations, *Phys. Rev. Mater.* 5 (2021) 013605.
- [8] N. Kvashin, A. Ostapovets, N. Anento, A. Serra, On the migration of $\{332\}\langle 110 \rangle$ tilt grain boundary in bcc metals and further nucleation of $\{112\}$ twin, *Comp. Mater. Sci.* 196 (2021) 110509.
- [9] N. Kvashin, N. Anento, D. Terentyev, A. Serra, $\{111\}$ tilt grain boundaries as barriers for slip transfer in bcc Fe, *Computational Materials Science* 203 (2022) 111044.
- [10] G. S. Was, Fundamentals of Radiation Materials Science, 2nd ed., Springer, New York, 2007.
- [11] M. A. Tschopp, K. N. Solanki, F. Gao, X. Sun, M. A. Khaleel, M. F. Horstemeyer, Probing grain boundary sink strength at the nanoscale: Energetics and length scales of vacancy and interstitial absorption by grain boundaries in α -Fe, *Phys. Rev. B* 85 (2012) 064108.
- [12] Z. Yang, L. Hu, D. Maroudas, K. D. Hammond, Helium segregation and transport behavior near $\langle 100 \rangle$ and $\langle 110 \rangle$ symmetric tilt grain boundaries in tungsten, *Journal of Applied Physics* 123 (2018) 225104.
- [13] T. Suzudo, H. Kaburaki, M. Yamaguchi, Modeling of the grain boundary segregation of helium in α -Fe, *Journal of Nuclear Materials* 417 (2011) 1102–1105. doi:<https://doi.org/10.1016/j.jnucmat.2011.02.014>.
- [14] W. Qin, A. K. Chauhan, J. A. Szpunar, Helium bubble nucleation at grain boundaries and its influence on intergranular fracture, *Philosophical Magazine* 99 (2019) 679–698. doi:[10.1080/14786435.2018.1551634](https://doi.org/10.1080/14786435.2018.1551634).
- [15] T. Suzudo, M. Yamaguchi, T. Tsuru, Atomistic modeling of He embrittlement at grain boundaries of α -Fe: a common feature over different grain boundaries, *Modelling and Simulation in Materials Science and Engineering* 21 (2013) 085013. doi:[10.1088/0965-0393/21/8/085013](https://doi.org/10.1088/0965-0393/21/8/085013).
- [16] J. X. Shang, X. D. Zhao, F. H. Wang, C. Y. Wang, H. B. Xu, Effects of Co and Cr on bcc Fe grain boundaries cohesion from first-principles study, *Computational Materials Science* 38 (2006) 217–222. doi:<https://doi.org/10.1016/j.commatsci.2006.02.010>.
- [17] Y. Yang, J. Ding, H. Zhang, P. Zhang, X. Mei, S. Huang, J. Zhao, Atomistic understanding of helium behaviors at grain boundaries in vanadium, *Computational Materials Science* 158 (2019) 296–306. doi:<https://doi.org/10.1016/j.commatsci.2018.11.036>.
- [18] K. Ito, H. Sawada, S. Ogata, First-principles study on the grain boundary embrittlement of bcc-Fe by Mn segregation, *Phys. Rev. Materials* 3 (2019) 013609. doi:[10.1103/PhysRevMaterials.3.013609](https://doi.org/10.1103/PhysRevMaterials.3.013609).
- [19] H. Beladi, G. S. Rohrer, The relative grain boundary area and energy distributions in a ferritic steel determined from three-dimensional electron backscatter diffraction maps, *Acta Materialia* 61 (2013) 1404–1412.
- [20] D. Terentyev, N. Anento, A. Serra, C. J. Ortiz, E. E. Zhurkin, Interaction of He and He-V clusters with self-interstitials and dislocations defects in bcc Fe, *Journal of Nuclear Materials* 458 (2015) 11–21.
- [21] Y. N. Osetsky, D. J. Bacon, Atomic-level interaction of an edge dislocation with localized obstacles in fcc and bcc metals, *IUTAM Symposium on Mesoscopic Dynamics of Fracture Process and Materials Strength* (2004) 193–202.

- [22] D. J. Bacon, Y. N. Osetsky, Modelling dislocation-obstacle interactions in metals exposed to an irradiation environment, *Materials Science and Engineering: A* (2005) 353–361.
- [23] G. Monnet, Multiscale modeling of precipitation hardening: Application to the Fe-Cr alloys, *Acta Materialia* 95 (2015) 302–311.
- [24] G. Monnet, Multiscale modeling of irradiation hardening: Application to important nuclear materials, *Journal of Nuclear Materials* 508 (2018) 609–627.
- [25] E. Orowan, Discussion on internal stresses, in: *Proc. Symp. Internal Stresses in Metals and Alloys*, London: The Institute of Metals, 1948, pp. 451–453.
- [26] M. R. Barnett, H. Wang, T. Guo, An Orowan precipitate strengthening equation for mechanical twinning in Mg, *International Journal of Plasticity* 112 (2019) 108–122.
- [27] Y. N. Osetsky, R. E. Stoller, Atomic-scale mechanisms of helium bubble hardening in iron, *Journal of Nuclear Materials* 465 (2015) 448–454.
- [28] G. Monnet, Y. N. Osetsky, D. J. Bacon, Mesoscale thermodynamic analysis of atomic-scale dislocation-obstacle interactions simulated by molecular dynamics, *Philosophical Magazine* 90 (2010) 1001–1018.
- [29] R. H. Richman, The diversity of twinning in body centred cubic structures, in: Reed-Hill, R.E., Hirth, J.P., Rogers, H.C. (eds.), *Deformation Twinning*, Gordon and Breach Sci. Publ., New York, 1964, pp. 237–271.
- [30] D. J. Bacon, U. F. Kocks, R. O. Scattergood, The effect of dislocation self-interaction on the Orowan stress, *The Philosophical Magazine: A Journal of Theoretical Experimental and Applied Physics* 28 (1973) 1241–1263. doi:10.1080/14786437308227997.
- [31] N. Anento, A. Serra, Interaction of a mobile {112} grain boundary with radiation induced defects in α -Fe: transformation of defects and impact on the shear-coupled grain boundary migration, *Comput. Mater. Sci.* 179 (2020) 109679.
- [32] A. Ostapovets, K. Kushnir, K. Mathis, F. Šiška, Interaction of migrating twin boundaries with obstacles in magnesium, *Metals* 11 (2021) 154.
- [33] A. Serra, D. J. Bacon, Interaction of a moving $\{10\bar{1}2\}$ twin boundary with perfect dislocations and loops in a hcp metal, *Philosophical Magazine* 90 (2010) 845–861.
- [34] S. Plimpton, Fast parallel algorithms for short-range molecular dynamics, *J. Comp. Phys.* 117 (1995) 1–19.
- [35] G. Ackland, M. Mendelev, D. Srolovitz, S. Han, A. Barashev, Development of an interatomic potential for phosphorus impurities in α -iron, *J. Phys.: Condens. Matter* 16 (2004) S2629–S2642.
- [36] D. Terentyev, N. Juslin, K. Nordlund, N. Sandberg, Fast three dimensional migration of He clusters in bcc Fe and Fe-Cr alloys, *Journal of Applied Physics* 105 (2009) 103509.
- [37] G. Bonny, R. C. Pasianot, D. Terentyev, L. Malerba, Iron chromium potential to model high-chromium ferritic alloys, *Philos. Mag.* 91 (2011) 1724–1746.
- [38] N. Kvashin, N. Anento, D. Terentyev, A. Serra, Atomic-level study on the interaction of plastic slip with $\Sigma 3\{112\}$ tilt grain boundary and $\{112\}$ twins in bcc metals, *Phys. Rev. Mater.* in preparation (2022).
- [39] P. Hirel, Atomsk: A tool for manipulating and converting atomic data files, *Comput. Phys. Comm.* 197 (2015) 212–219.
- [40] A. Stukowski, Visualization and analysis of atomistic simulation data with OVITO – the open visualization tool, *Modelling Simul. Mater. Sci. Eng.* 18 (2010) 015012.